Influence of electron–phonon interaction on the properties of transport through double quantum dot with ferromagnetic leads*

Luo Kan(罗 侃), Wang Fa-Qiang(王发强)†, Liang Rui-Sheng(梁瑞生), and Ren Zhen-Zhen(任珍珍)

Laboratory of Nanophotonic Functional Materials and Devices (SIPSE), and Laboratory of Quantum Engineering and Quantum Materials, South China Normal University, Guangzhou 510006, *China*

(Received 22 April 2014; revised manuscript received 22 May 2014; published online 20 August 2014)

Electronic transport through a vibrating double quantum dot (DQD) in contact with noncollinear ferromagnetic (FM) leads is investigated. The state transition between the two dots of the DQD is excited by an AC microwave driving field. The corresponding currents and differential conductance are calculated in the Coulomb blockade regime by means of the Born–Markov master equation. It is shown that the interplay between electrons and phonons gives rise to phonon-assisted tunneling resonances and Franck–Condon blockade under certain conditions. In noncollinear magnetic configurations, spin-blockade effects are also observed, and the angle of polarization has some influence on the transport characteristics.

Keywords: electron–phonon, spin-polarized transport, negative differential conductance

PACS: 71.38.–k, 72.25.–b **DOI:** 10.1088/1674-1056/23/10/107103

1. Introduction

With the development of nanotechnology, nanomechanical systems are drawing considerable interest because they provide a good platform for studying electron transport phenomena in the sphere of modern mesoscopic physics. One of the most interesting nanomechanical systems is composed of two quantum dots connected serially or in parallel by leads. In a double quantum dot[1] system it is easy to change both the splitting of energy levels and the rate of the electron tunneling to the leads by varying the gate voltage. The transport properties of the DQD system have been extensively studied in recent years, both theoretically[2–8] and experimentally.[9–14] Both electron–electron interaction, which gives rise to Coulomb blockade, and strong electron–phonon[15–19] (EP) coupling often influence the transport through the DQD system. An intriguing phenomenon known as the Franck–Condon effect[20–22] has been observed in suspended carbon nanotubes (CNTs) due to the EP coupling. The Franck–Condon blockade can lead to a negative differential conductance[23–25] when the bias voltage exceeds the phonon frequency.

In the past few years, spin-dependent transport through nanoelectromechanical systems has been a hot topic. Typical examples include quantum shuttles,[26–28] spin valves,[29–31] and double-dot structures.[32–34] It has been demonstrated that these structures are ideal systems for studying the fundamental interplay between electrons and spins. A typical system is a DQD coupled to two ferromagnetic leads that in most cases have collinear magnetization directions and the same spin-polarization. Compared with the collinear case, richer physical effects have been obtained in the noncollinear case.[35,36] For example, both the exchange effect and effective field induced by a nonlocal interface exchange have to be taken into account. It has been found that the exchange field increases the differential conductance for DQD coupled to FM with a noncollinear alignment of magnetizations. Moreover, the exchange effect has several potential applications in quantum information processing because of the convenience of controlling magnetic fields in arbitrary directions.

In this paper, we study the spin-dependent transport properties of a DQD system connected to leads with arbitrary polarization directions. In the F-DQD-F system, a vibrational mode is coupled to each dot. There is a splitting of energy levels between the two dots of the DQD, and we apply an AC microwave field with a frequency of $\omega_{\rm d}$ to excite the state transition in the DQD. As shown below, some interesting phenomena, including negative differential conductance and phonon-assisted tunneling, are observed in the $\mathrm{d}I/\mathrm{d}V$ characteristic curves. This is different from a recently published article (Ref. [2]) that has shown the differential conductance disappearing in the case of asymmetric energy levels.

The rest of this paper is organized as follows. In Section 2, we present the F-DQD-F model and derive its effective Hamiltonian. In Section 3, we employ an efficient particle-number-resolved master equation approach to derive a general formalism for both the spin-dependent currents and the differential conductance. The numerical results are presented in Section 4, followed by the conclusion in Section 5.

2. Model description

A schematic view of the system under study is shown in Fig. 1. The total Hamiltonian of the whole system is given by

*Project supported by the National Natural Science Foundation of China (Grant No. 61275059).

†Corresponding author. E-mail: fqwang@scnu.edu.cn

© 2014 Chinese Physical Society and IOP Publishing Ltd

$$H_{\rm tot} = H_{\rm leads} + H_{\rm DQD} + H_{\rm R} + H_{\rm T} + H_{\rm int}, \tag{1}$$

where

$$H_{\rm leads} = \sum_{\alpha k\sigma} \varepsilon_{\alpha k} c^{\dagger}_{\alpha k\sigma} c_{\alpha k\sigma}, \tag{2}$$

describes the ferromagnetic electrodes.[19] $c_{{\rm l}k\sigma}\left(c^{\dagger}_{{\rm l}k\sigma}\right)$ is the electron annihilation (creation) operator with momentum k, and spin $\sigma =\uparrow$ or $\downarrow$.

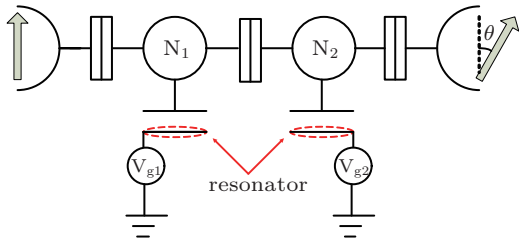


Fig. 1. (color online) Schematic diagram of a DQD connected to ferromagnetic electrodes. Under each quantum dot, a nanomechanical resonator (NMR) and another static plate form a capacitor, which provides a capacitive coupling between the oscillating NMR and the DQD. The energy level of each dot is tunable by varying the gate voltage $V_{\rm g}$ applied to the dot through the capacitor. In addition, two localized states in the DQD, with energy level difference $\hbar\omega_0$ are driven by an AC microwave field.

The FM electrode is characterized by the spin-dependent density of states $g_{\alpha\sigma}(\omega)$. Because the density of states is energy-independent, the FM polarization of the electrodes can be simply determined by a parameter, which satisfies $0 \le p_\alpha \le 1$ ($p_\alpha = 0$ corresponds to metal electrodes, $p_\alpha = 1$ corresponds to half- metallic electrodes).

The Hamiltonian of the DQD is given by

$$H_{\rm DQD} = \sum_{\sigma}\left[\frac{\omega_0}{2}\sigma_{z\sigma} + \Omega\sigma_{x\sigma} + \Omega_0\cos(\omega_{\rm d}t)\,\sigma_{x\sigma}\right], \tag{3}$$

which is driven by a microwave field; $\sigma_{z\sigma} = a^{\dagger}_{2\sigma}a_{2\sigma} - a^{\dagger}_{1\sigma}a_{1\sigma}$ and $\sigma_{x\sigma} = a^{\dagger}_{2\sigma}a_{1\sigma} + a^{\dagger}_{1\sigma}a_{2\sigma}$ are the Pauli matrices with $a^{\dagger}_{1\sigma}\left(a^{\dagger}_{2\sigma}\right)$ the electron annihilation (creation) operator in the left (right) quantum dot and with spin σ; and Ω is the coupling strength between the two dots, in the third term Ω_0 and $\omega_{\rm d}$, respectively, denote the driving amplitude and frequency of the applied microwave field.

The Hamiltonian for the resonator is given by

$$H_{\rm R} = \omega_{\rm m} b^{\dagger} b, \tag{4}$$

where the eigenmode is described by a quantum harmonic resonator with the bosonic creation operator $b^{\dagger}$ and annihilation operator b.

We chose a symmetric electron–phonon coupling constant $\lambda_L = \lambda_{\rm R} = \lambda$, so the coupling between the phonon and the electron in the DQD is described by

$$H_{\rm int} = \lambda\sum_{\sigma}\left(a^{\dagger}_{1\sigma}a_{1\sigma} + a^{\dagger}_{2\sigma}a_{2\sigma}\right)\left(b^{\dagger} + b\right), \tag{5}$$

where the electromechanical coupling strength is $\lambda = \eta\omega_{\rm m}$, and the tunneling Hamiltonian is

$$\begin{aligned} H_{\rm T} = \sum_{k\sigma}\Bigg(&\Omega_{{\rm l}k\sigma}c^{\dagger}_{{\rm l}k\sigma}a_{1\sigma} + \Omega_{{\rm r}k\sigma}c^{\dagger}_{{\rm r}k\sigma}a_{2\sigma}\cos\frac{\theta}{2} \\ &- \sigma\Omega_{{\rm r}k\bar{\sigma}}c^{\dagger}_{{\rm r}k\bar{\sigma}}a_{2\sigma}\sin\frac{\theta}{2} + {\rm h.c.}\Bigg), \end{aligned} \tag{6}$$

where $\Omega_{{\rm l}k({\rm r}k)}$ is the coupling strength between the QD and the left lead (right lead).

Because the dynamics of the DQD, the NMR, and the coupling between them have different time scales, it is difficult to directly analyze the coupled system. So, we first eliminate the coupling between the DQD and the NMR with a Lang–Firsov transformation[37–39] $U_{\rm S} = \sum_{\sigma} {\rm e}^{\eta\left(a^{\dagger}_{1\sigma}a_{1\sigma} + a^{\dagger}_{2\sigma}a_{2\sigma}\right)\left(b^{\dagger} - b\right)}$ on the whole system, and the transformed Hamiltonian is given by

$$\begin{aligned} H' &= U_{\rm S}H_{\rm tot}U^{\dagger}_{\rm S} \\ &= \sum_{\alpha k\sigma}\varepsilon_{\alpha k}c^{\dagger}_{\alpha k\sigma}c_{\alpha k\sigma} \\ &\quad + \sum_{\sigma}\left[\left(\frac{\omega_0}{2} - \eta^2\omega_{\rm m}\right)a^{\dagger}_{2\sigma}a_{2\sigma} - \left(\frac{\omega_0}{2} + \eta^2\omega_{\rm m}\right)a^{\dagger}_{1\sigma}a_{1\sigma}\right] \\ &\quad + \left(\Omega + \Omega_0\cos(\omega_{\rm d}t)\right)\sum_{\sigma}\left(\sigma_{\dagger\sigma}B^{\dagger}B + \sigma_{-\sigma}B^{\dagger}B\right) \\ &\quad + \omega_{\rm m}b^{\dagger}b + \sum_{k}\Bigg\{\Omega_{{\rm l}k\uparrow}c^{\dagger}_{{\rm l}k\uparrow}a_{1\uparrow}B + \Omega_{{\rm l}k\downarrow}c^{\dagger}_{{\rm l}k\downarrow}a_{1\downarrow}B \\ &\quad + \Omega_{{\rm r}k\uparrow}\cos\frac{\theta}{2}c^{\dagger}_{{\rm r}k\uparrow}a_{2\uparrow}B - \Omega_{{\rm r}k\downarrow}\sin\frac{\theta}{2}c^{\dagger}_{{\rm r}k\downarrow}a_{2\uparrow}B \\ &\quad + \Omega_{{\rm r}k\downarrow}\cos\frac{\theta}{2}c^{\dagger}_{{\rm r}k\downarrow}a_{2\downarrow}B + \Omega_{{\rm r}k\uparrow}\sin\frac{\theta}{2}c^{\dagger}_{{\rm r}k\uparrow}a_{2\downarrow}B + {\rm h.c.}\Bigg\}, \end{aligned} \tag{7}$$

where ω_0 denotes the energy-level splitting of the DQD, $\sigma_{+\sigma} = \sigma^{\dagger}_{-\sigma} = a^{\dagger}_{2\sigma}a_{1\sigma}$ is the ladder operator, and $B = \exp\left[-\eta\left(b^{\dagger} - b\right)\right]$.

In the next step, we employ a unitary transform

$$U_{\rm R} = \exp\left(-{\rm i}\frac{\omega_{\rm d}}{2}\sum_{\sigma}\sigma_{z\sigma}t\right)$$

to change the Hamiltonian to a rotating frame. Under rotating wave approximation, the resulting Hamiltonian is given by

$$\begin{aligned} \tilde{H} &= {\rm i}\frac{{\rm d}U^{\dagger}_{\rm R}}{{\rm d}t}U_{\rm R} + U^{\dagger}_{\rm R}H'U_{\rm R} \\ &= H_{\rm sys} + \sum_{\alpha k\sigma}\varepsilon_{\alpha k}c^{\dagger}_{\alpha k\sigma}c_{\alpha k\sigma} \\ &\quad + \sum_{k}\Bigg\{\Omega_{{\rm l}k}c^{\dagger}_{{\rm l}k\uparrow}a_{1\uparrow}B\exp\left({\rm i}\frac{\omega_{\rm d}}{2}t\right) + \Omega_{{\rm l}k}c^{\dagger}_{{\rm l}k\downarrow}a_{1\downarrow}B\exp\left({\rm i}\frac{\omega_{\rm d}}{2}t\right) \\ &\quad + \Omega_{{\rm r}k}\cos\frac{\theta}{2}c^{\dagger}_{{\rm r}k\uparrow}a_{2\uparrow}B\exp\left(-{\rm i}\frac{\omega_{\rm d}}{2}t\right) \\ &\quad - \Omega_{{\rm r}k}\sin\frac{\theta}{2}c^{\dagger}_{{\rm r}k\downarrow}a_{2\uparrow}B\exp\left(-{\rm i}\frac{\omega_{\rm d}}{2}t\right) \\ &\quad + \Omega_{{\rm r}k}\cos\frac{\theta}{2}c^{\dagger}_{{\rm r}k\downarrow}a_{2\downarrow}B\exp\left(-{\rm i}\frac{\omega_{\rm d}}{2}t\right) \\ &\quad + \Omega_{{\rm r}k}\sin\frac{\theta}{2}c^{\dagger}_{{\rm r}k\uparrow}a_{2\downarrow}B\exp\left(-{\rm i}\frac{\omega_{\rm d}}{2}t\right) + {\rm h.c.}\Bigg\}, \end{aligned} \tag{8}$$

with

$$H_{\rm sys} = \sum_{\sigma}\left[-\left(\frac{\Delta}{2}+\eta^2\omega_{\rm m}\right)a^{\dagger}_{2\sigma}a_{2\sigma} + \left(\frac{\Delta}{2}-\eta^2\omega_{\rm m}\right)a^{\dagger}_{1\sigma}a_{1\sigma}\right] + \omega_{\rm m}b^{\dagger}b+\left(\Omega+\frac{\Omega_0}{2}\right)\sum_{\sigma}\sigma_{x\sigma}B^{\dagger}B, \quad (9)$$

where $\Delta=\omega_{\rm d}-\omega_0$ is the driving frequency detuning the microwave field from the transition frequency of the DQD.

3. Formalism

In this section, we consider the DQD weakly coupled to ferromagnetic leads in the Coulomb blockade regime, and use the particle-number-resolved master equation approach[40,41] within the Born–Markov approximation for the calculation of the spin-dependent currents and differential conductance.

3.1. Born–Markov master equation

The non-equilibrium dynamics of the coupled NMR-DQD system can be described by the master equation for the reduced density matrix, which can be approximated as $\rho_{\rm tot}(t)\approx\rho_{\rm d}(t)\otimes\rho_{\rm ph}\otimes\rho_{\rm leads}$. By tracing out the leads and the phonons, the DQD density matrix can be obtained:

$$\begin{aligned}\frac{\rm d}{{\rm d}t}\rho_{\rm d}(t) =& -{\rm i}\sum_{\sigma}\left[-\left(\frac{\Delta}{2}+\eta^2\omega_{\rm m}\right)a^{\dagger}_{2\sigma}a_{2\sigma} + \left(\frac{\Delta}{2}-\eta^2\omega_{\rm m}\right)a^{\dagger}_{1\sigma}a_{1\sigma},\rho_{\rm d}\right]\\ &-{\rm i}\left(\frac{\Omega_0}{2}+\Omega\right)M\sum_{\sigma}[\sigma_{x\sigma},\rho_{\rm d}]\\ &+\sum_{\sigma}\left[W^{\sigma}_{10}\mathcal{D}[a_{1\sigma}]\rho_{\rm d}+W^{\sigma}_{01}\mathcal{D}\left[a^{\dagger}_{1\sigma}\right]\rho_{\rm d}\right.\\ &\left.+W^{\sigma}_{02}\mathcal{D}\left[a^{\dagger}_{2\sigma}\right]\rho_{\rm d}+W^{\sigma}_{20}\mathcal{D}[a_{2\sigma}]\rho_{\rm d}\right], \quad (10)\end{aligned}$$

where the notation $\mathcal{D}$ is defined as

$$\mathcal{D}[A]\rho = A\rho A^{\dagger}-\frac{1}{2}\left[A^{\dagger}A\rho+\rho A^{\dagger}A\right],$$

while A is an arbitrary operator, and $M={\rm Tr}_{\rm ph}\left(\rho_{\rm ph}B^{\dagger}B\right)=\left\langle B^{\dagger}B\right\rangle$ is the time-independent correlation function. For equilibrated phonons,

$$M = \left(1-{\rm e}^{-\beta_{\rm bos}\omega_{\rm m}}\right)^2{\rm e}^{-\eta^2}\sum_{n=0}^{\infty}{\rm e}^{-\beta_{\rm bos}\omega_{\rm m}n}{\rm L}_n\left(\eta^2\right) \times\sum_{m=0}^{\infty}{\rm e}^{-\beta_{\rm bos}\omega_{\rm m}m}{\rm L}_{\rm m}\left(\eta^2\right),$$

where $\rm L_n$ are Laguerre polynomials, $g=\eta^2$ and $\beta_{\rm ph}$ is the inverse temperature of the phonon, and W^{σ}_{0i} and W^{σ}_{i0} represent the tunneling rates between the leads and the i-th dot $(i=1,2)$

$$W^{\sigma}_{01} = \int_{-\infty}^{\infty}\frac{{\rm d}\omega}{2\pi}\Gamma_{\rm l\sigma}f_{\rm l}\left(-\frac{\omega_0}{2}-\eta^2\omega_{\rm m}+\omega\right)G(\omega),$$

$$W^{\sigma}_{10} = \int_{-\infty}^{\infty}\frac{{\rm d}\omega}{2\pi}\Gamma_{\rm l\sigma}\left[1-f_{\rm l}\left(-\frac{\omega_0}{2}-\eta^2\omega_{\rm m}+\omega\right)\right]F(\omega),$$

$$W^{\sigma}_{02} = \int_{-\infty}^{\infty}\frac{{\rm d}\omega}{2\pi}\left(\Gamma_{\rm r\sigma}\cos^2\frac{\theta}{2}+\Gamma_{\rm r\bar{\sigma}}\sin^2\frac{\theta}{2}\right) \times f_{\rm r}\left(\frac{\omega_0}{2}-\eta^2\omega_{\rm m}+\omega\right)G(\omega),$$

$$W^{\sigma}_{20} = \int_{-\infty}^{\infty}\frac{{\rm d}\omega}{2\pi}\left(\Gamma_{\rm r\sigma}\cos^2\frac{\theta}{2}+\Gamma_{\rm r\bar{\sigma}}\sin^2\frac{\theta}{2}\right) \times\left[1-f_{\rm r}\left(\frac{\omega_0}{2}-\eta^2\omega_{\rm m}+\omega\right)\right]F(\omega),$$

where $\Gamma_{\alpha\sigma}=2\pi g_{\alpha\sigma}|\Omega_{\alpha}|^2$ denotes the spin-dependent tunneling-induced level broadening in the case of a collinear configuration. In addition $\Gamma_{\rm l\sigma}=\Gamma_0(1+\sigma_z p)$ and $\Gamma_{\rm r\sigma}=\Gamma_0(1\pm\sigma_z p)$ where sign $+$ $(-)$ stands for the parallel (antiparallel) configuration of the FM leads, and $\Gamma_0=\left(\Gamma_{\alpha\uparrow}+\Gamma_{\alpha\downarrow}\right)/2$ denotes tunneling broadening without internal magnetization, and $f_{\alpha}(x)=\left[{\rm e}^{\beta_{\rm el}(x-\mu_{\alpha})}+1\right]^{-1}$ is the Fermi function of lead α held at inverse temperature $\beta_{\rm el}$ and chemical potential μ_{α}. After using the Fourier transform of the bosonic correlation function $F(\tau)=F(t-t')=\left\langle B(t)B^{\dagger}(t')\right\rangle F,(\omega)$ can be calculated exactly[16]

$$F(\omega) = \sum_{n=-\infty}^{\infty}\exp\left[-g(1+2N)\right]\left(\frac{1+N}{N}\right)^{n/2} \times{\rm I}_n\left(2g\sqrt{N(1+N)}\right)2\pi\delta(\omega+n\omega_{\rm m}),$$

where $\rm I_n$ is the modified Bessel function of the first kind, and $N=\left({\rm e}^{\beta_{\rm ph}\omega_{\rm m}}-1\right)^{-1}$ is the Bose distribution with inverse temperature $\beta_{\rm ph}$. Note that we set $\hbar=k_{\rm B}=1$.

In the stationary case, we assume that the DQD is in the strong Coulomb repulsion (including interdot and intradot cases), such that only one single electron is allowed in the DQD. The occupation probabilities of the DQD are $\rho_0=\langle 0|\langle 0|\rho_{\rm d}|0\rangle|0\rangle$, $\rho_{1\sigma}=\langle 0|\langle\sigma|\rho_{\rm d}|\sigma\rangle|0\rangle$, and $\rho_{2\sigma}=\langle\sigma|\langle 0|\rho_{\rm d}|0\rangle|\sigma\rangle$ with $|\sigma\rangle=|\uparrow\rangle$ (or $|\downarrow\rangle$).

3.2. Rate equations for the density matrix

From the master equation (10), a set of rate equations for the corresponding density matrix $\rho^{(n)}_{ij\sigma}(t)$ can be obtained. This density matrix gives the probability of finding n spin σ electrons at the right lead by time t The indices $i,j=\{0,1,2\}$ denote the different possibilities of occupation of the states of the dots, namely: $\rho^{(n)}_{00}$ is the probability of finding both dots unoccupied, $\rho^{(n)}_{11\sigma}$, $\rho^{(n)}_{22\sigma}$ are the probabilities of finding the first and the second dots occupied, respectively; and, $\rho^{(n)}_{12\sigma}=\rho^{*(n)}_{21\sigma}$ denotes the off-diagonal density matrix elements (the "coherencies"). The rate equations can be written as[42,43]

$$\begin{aligned}\frac{\rm d}{{\rm d}t}\rho^{(n)}_{00} =& -\sum_{\sigma}(W^{\sigma}_{01}+W^{\sigma}_{02})\rho^{(n)}_{00}+\sum_{\sigma}W^{\sigma}_{10}\rho^{(n)}_{11\sigma}\\ &+\sum_{\sigma}W^{\sigma}_{20}\rho^{(n-1)}_{22\sigma}, \quad (11)\\ \frac{\rm d}{{\rm d}t}\rho^{(n)}_{11\sigma} =& -{\rm i}\left(\Omega+\frac{\Omega_0}{2}\right)M\left[\rho^{(n)}_{21\sigma}-\rho^{(n)}_{12\sigma}\right]\end{aligned}$$

$$+W_{01}^{\sigma}\rho_{00}^{(n+1)}-(W_{10}^{\sigma}+W_{02}^{\sigma})\rho_{11\sigma}^{(n)}, \quad (12)$$

$$\frac{\mathrm{d}}{\mathrm{d}t}\rho_{22\sigma}^{(n)} = -\mathrm{i}\left(\Omega+\frac{\Omega_0}{2}\right)M\left[\rho_{12\sigma}^{(n)}-\rho_{21\sigma}^{(n)}\right] +W_{02}^{\sigma}\rho_{00}^{(n+1)}-(W_{20}^{\sigma}+W_{01}^{\sigma})\rho_{22\sigma}^{(n)}, \quad (13)$$

$$\frac{\mathrm{d}}{\mathrm{d}t}\rho_{12\sigma}^{(n)} = -\mathrm{i}\Delta\rho_{12\sigma}^{(n)}-\mathrm{i}\left(\Omega+\frac{\Omega_0}{2}\right)M\left[\rho_{22\sigma}^{(n)}-\rho_{11\sigma}^{(n)}\right] -\frac{1}{2}(W_{01}^{\sigma}+W_{02}^{\sigma}+W_{10}^{\sigma}+W_{20}^{\sigma})\rho_{12\sigma}^{(n)}, \quad (14)$$

$$\frac{\mathrm{d}}{\mathrm{d}t}\rho_{21\sigma}^{(n)} = \mathrm{i}\Delta\rho_{21\sigma}^{(n)}-\mathrm{i}\left(\Omega+\frac{\Omega_0}{2}\right)M\left[\rho_{11\sigma}^{(n)}-\rho_{22\sigma}^{(n)}\right] -\frac{1}{2}(W_{01}^{\sigma}+W_{02}^{\sigma}+W_{10}^{\sigma}+W_{20}^{\sigma})\rho_{21\sigma}^{(n)}. \quad (15)$$

Equations (11)–(15) allow one to calculate the particle current from

$$N(t)=\sum_n n\left[\rho_{00}^{(n)}(t)+\rho_{11\uparrow}^{(n)}(t)+\rho_{11\downarrow}^{(n)}(t)+\rho_{22\uparrow}^{(n)}(t)+\rho_{22\downarrow}^{(n)}(t)\right],$$

which gives the total number of electrons at the right electrode at time t. The total charge and spin-dependent current flowing in the system are given by

$$I_{\mathrm{R}}(t)=e\frac{\mathrm{d}N(t)}{\mathrm{d}t}=-e\sum_{\sigma}[W_{02}^{\sigma}\rho_0(t)-W_{20}^{\sigma}\rho_{2\sigma}(t)], \quad (16)$$

$$I_{\mathrm{R}}^{\uparrow}(t)=-e\sum_{\sigma}\left[W_{02}^{\uparrow}\rho_0(t)-W_{20}^{\uparrow}\rho_{2\uparrow}(t)\right], \quad (17)$$

$$I_{\mathrm{R}}^{\downarrow}(t)=-e\sum_{\sigma}\left[W_{02}^{\downarrow}\rho_0(t)-W_{20}^{\downarrow}\rho_{2\downarrow}(t)\right], \quad (18)$$

when

$$\frac{\mathrm{d}}{\mathrm{d}t}\rho_{ij\sigma}^{(n)}=0.$$

With the normalization condition $\rho_0+\sum_{\sigma}\rho_{1\sigma}+\sum_{\sigma}\rho_{2\sigma}=1$ the steady-state solution of Eqs. (11)–(15) is given by

$$\begin{aligned}
\rho_{1\sigma} &= X_{\sigma}\rho_0,\\
\rho_{2\sigma} &= \frac{\left[W_{02}^{\sigma}+W_{10}^{\sigma}+(\Omega+\Omega_0/2)^2\Lambda_{\sigma}\right]X_{\sigma}-W_{01}^{\sigma}}{(\Omega+\Omega_0/2)^2\Lambda_{\sigma}}\rho_0,\\
\rho_0 &= (\Omega+\Omega_0/2)^2\Lambda_{\uparrow}\Lambda_{\downarrow}\\
&\quad\times\left\{(\Omega+\Omega_0/2)^2\Lambda_{\uparrow}\Lambda_{\downarrow}\left(X_{\uparrow}\dagger X_{\downarrow}\dagger 1\right)\right.\\
&\quad+\left[W_{02}^{\uparrow}+W_{10}^{\uparrow}+(\Omega+\Omega_0/2)^2\Lambda_{\uparrow}\right]\Lambda_{\downarrow}X_{\uparrow}\\
&\quad+\left[W_{02}^{\downarrow}+W_{10}^{\downarrow}+(\Omega+\Omega_0/2)^2\Lambda_{\downarrow}\right]\\
&\quad\left.\times\Lambda_{\uparrow}X_{\downarrow}-W_{01}^{\uparrow}\Lambda_{\downarrow}-W_{01}^{\downarrow}\Lambda_{\uparrow}\right\}^{-1},
\end{aligned}$$

where

$$\Lambda_{\sigma}=\frac{(W_{01}^{\sigma}+W_{02}^{\sigma}+W_{10}^{\sigma}+W_{20}^{\sigma})M^2}{\Delta^2+(W_{01}^{\sigma}+W_{02}^{\sigma}+W_{10}^{\sigma}+W_{20}^{\sigma})^2/4},$$

$$X_{\sigma}=\frac{(\Omega+\Omega_0/2)^2\Lambda_{\sigma}W_{02}^{\sigma}+\left[W_{01}^{\sigma}+W_{20}^{\sigma}+(\Omega+\Omega_0/2)^2\Lambda_{\sigma}\right]W_{01}^{\sigma}}{\left[W_{01}^{\sigma}+W_{20}^{\sigma}+(\Omega+\Omega_0/2)^2\Lambda_{\sigma}\right]\left[W_{02}^{\sigma}+W_{10}^{\sigma}+(\Omega+\Omega_0/2)^2\Lambda_{\sigma}\right]-(\Omega+\Omega_0/2)^4\Lambda_{\sigma}^2}.$$

4. Currents and differential conductance

In the following, we present results on the currents and differential conductance through the DQD system. For the sake of simplicity, we assume both leads have the same spin polarization (i.e., $p_{\mathrm{L}}=p_{\mathrm{R}}$), and we choose $\beta_{\mathrm{el}}=\beta_{\mathrm{ph}}=10\omega_{\mathrm{m}}$ corresponding to a low temperatures for the electron and boson. For the chemical potentials we take $\mu_{\mathrm{L}}=V/2$ and $\mu_{\mathrm{R}}=-V/2$.

(i) We study the relation between transport properties and the electron–phonon coupling. In Figs. 2(a)–2(f), the spin-down, spin-up, and total currents are plotted as functions of bias voltage V for different electron–phonon couplings g. Subfigures 2(a)–2(c) correspond to the P configuration, and subfigures 2(d)–2(f) correspond to the AP configuration. First, in the P configuration, the spin-down, spin-up, and total currents all decrease with increasing electron–phonon coupling g for a fixed applied bias. In the absence of electron–phonon coupling, the I–V curves show a big step, and in the region $-2<V<-1$ the currents increase sharply due to resonant tunneling. In the presence of electron–phonon coupling, the currents decrease somewhat, and these I–V curves show a series of Franck–Condon steps[44,45] that can be viewed as the signatures of phonon-assisted tunneling. In addition, when the electron–phonon coupling is strong and $V<-4$, these I–V curves clearly show the famous negative differential conductance phenomenon first and then the phonon-assisted tunneling features for a large negative applied bias voltage. This happens because, for a negative bias voltage $-6<V<-4$, the currents decrease due to the Franck–Condon blockade (phonons absorb energy from the tunneling electron); when $V<-6$ the process of the phonons emitting energy to a tunneling electron plays a primary role to assist tunneling. Second, in the AP configuration, the analyses of all I–V curves are almost the same as in the P configuration, the only difference is the spin blockade that makes all the spin currents decrease in the AP configuration. Third, via the $\mathrm{d}I/\mathrm{d}V$ curve shown in Fig. 3, the current transport can be seen in more detail. There are many peaks located at $V=\pm 2n$ $(n=1,2,\ldots)$ in the differential conductance. The highest peak corresponds to the cotunneling, other positive peaks correspond to the phonon-assisted tunneling, and the negative peaks correspond to the Franck–Condon blockade.

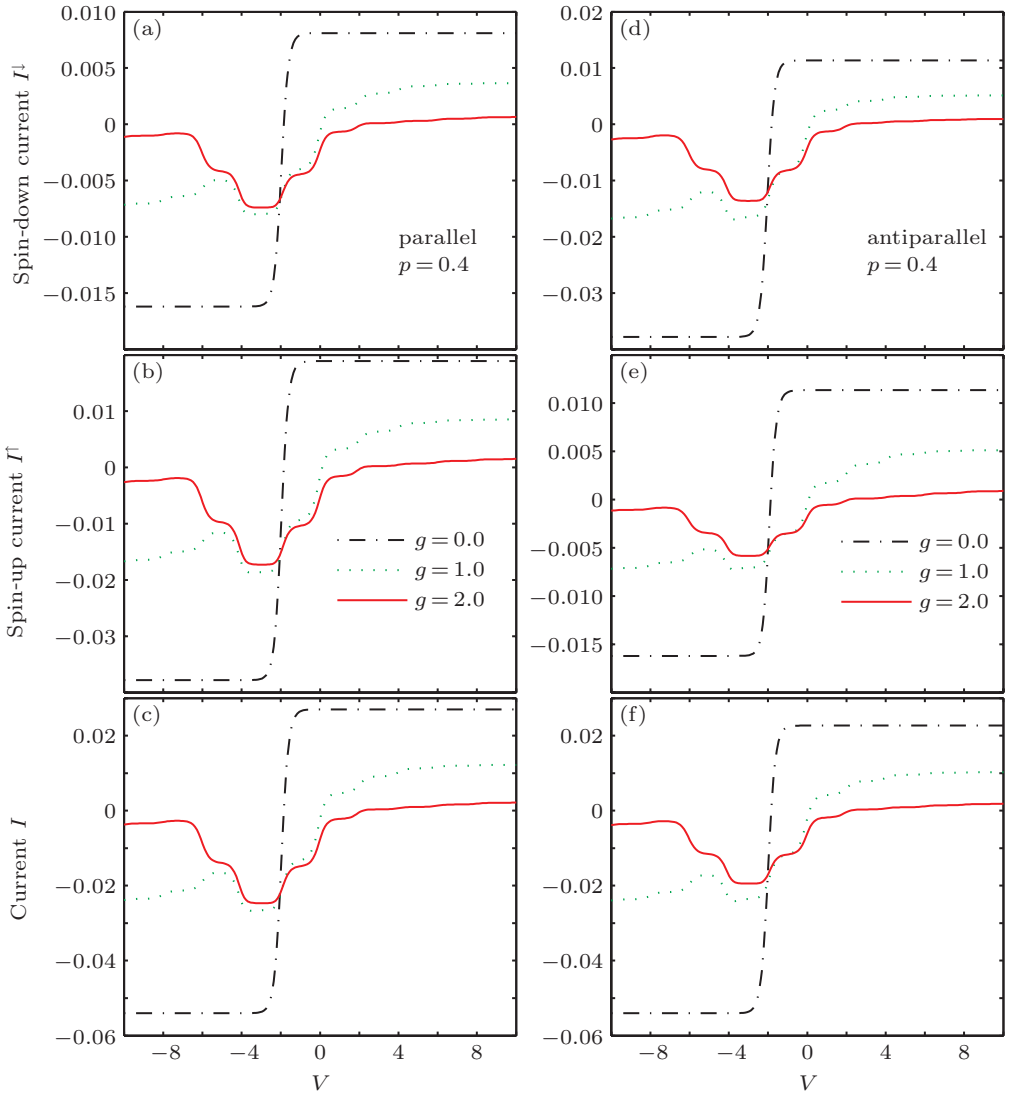


Fig. 2. (color online) Currents $I/e\omega_{\rm m}$ as a function of bias voltage V for different values of electron–phonon coupling g. Subfigures (a)–(c) show, respectively, the spin-down, spin-up, and total current for the parallel (P) configuration, and those in panels (d)–(f) are the corresponding currents for the antiparallel (AP) configuration. The parameters are $\Gamma_0 = 0.1$, $\omega_{\rm m} = 1$, $\omega_0 = 2$, $\Omega = 0.2$, $\Omega_0 = 2$, $p = 0.4$, and the driving detuning $\Delta = \omega_{\rm d} - \omega_0 = -1$.

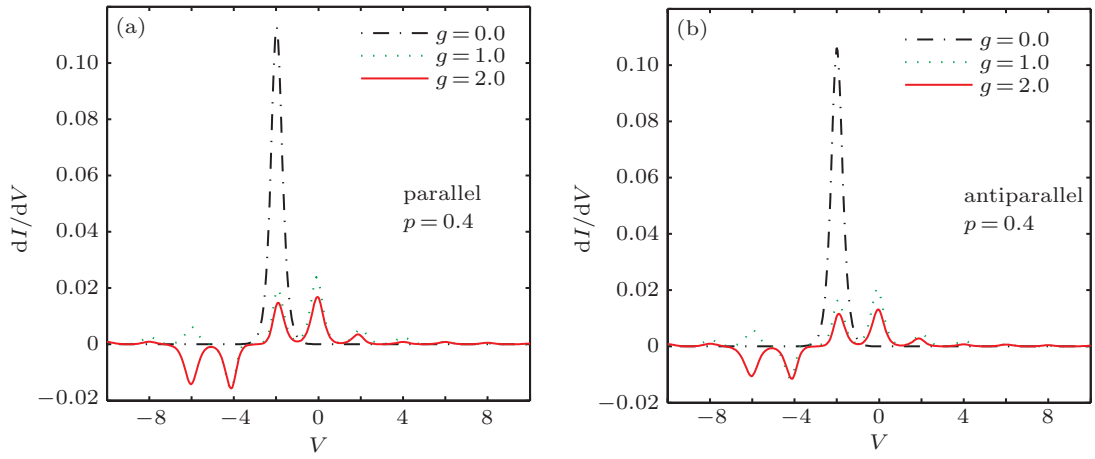


Fig. 3. (color online) Differential conductance dI/dV as a function of bias voltage V in the (a) P and (b) AP configurations for different electron–phonon couplings g. The parameters are the same as those in Fig. 2.

(ii) We discuss the relationship between transport properties and spin polarization. In Figs. 4(a)–4(f), the spin-down, spin-up, and total currents are plotted as a function of bias voltage V for different spin polarizations p. Subfigures (a)–(c) correspond to the P configuration, and panels (d)–(f) correspond to the AP configuration. First, in the P configuration, it can be seen that the sign of the currents depends on the bias voltage V. The spin-down current decreases with increasing spin polarization, but the spin-up current is just the opposite. For a fixed spin polarization, the increase of spin-up current is equal to the reduction of spin-down current, so the total current is unchanging. Second, in the AP configuration, these currents all decrease with increasing spin polarization for positive applied bias. This happens because the electron spin blockade caused by the spin accumulation becomes bigger with increasing spin polarization. For a small negative applied bias, the spin-down current first increases and then decreases, but the total current decreases as long as the spin polarization increases. When the negative applied bias is large, the spin-down and total current increase with increasing spin polarization. The spin-up current decreases with increasing spin polarization, whether the negative applied bias is small or large. For clarity, we present the differential conductance $\mathrm{d}I/\mathrm{d}V$ as a function of the bias voltage for different spin polarizations in Fig. 5. It can be seen that in the P configuration, the differential conductance has nothing to do with the spin polarization, while in the AP configuration the peaks of differential conductance step down with increasing spin polarization.

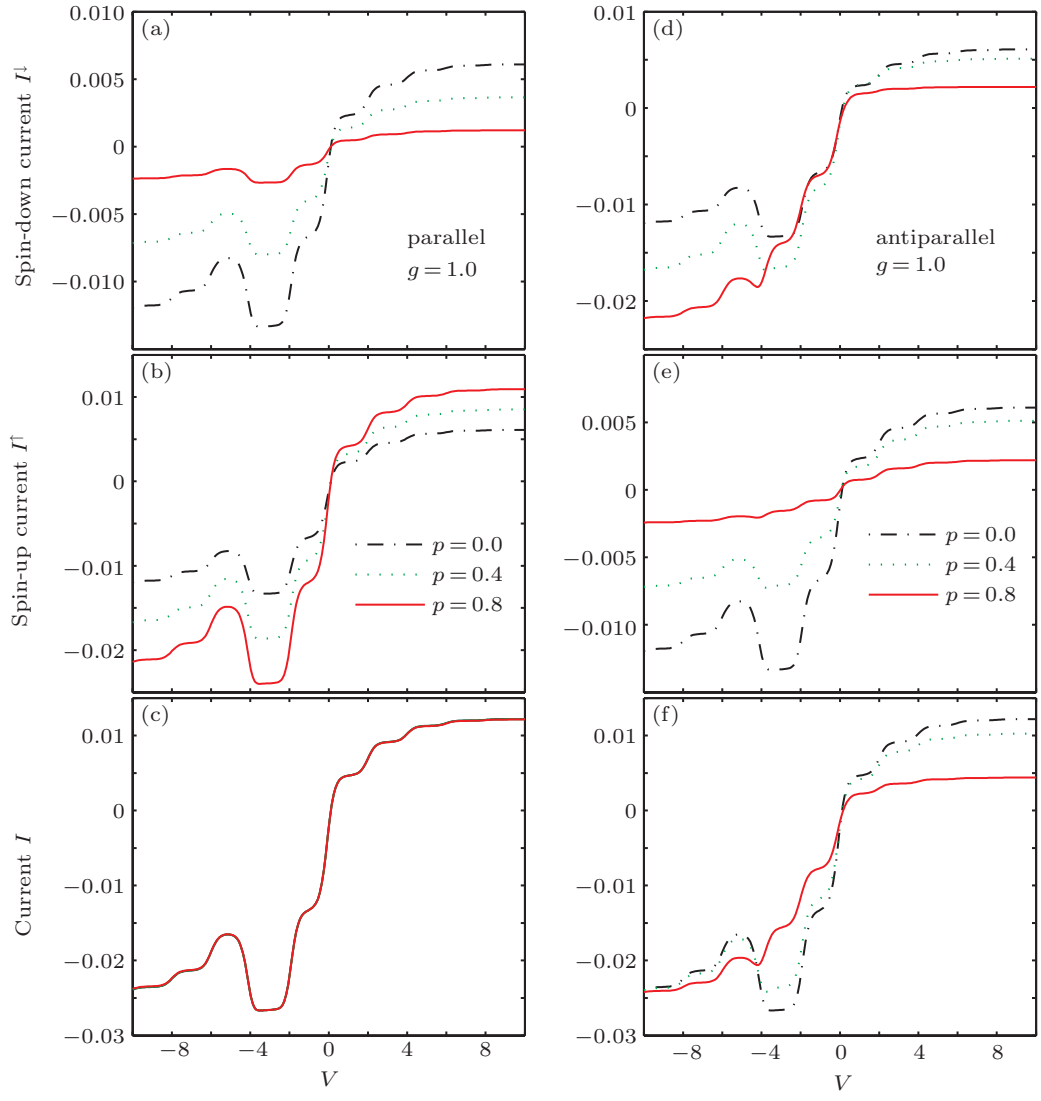


Fig. 4. (color online) Currents $I/e\omega_{\mathrm{m}}$ versus bias voltage V for different spin polarizations p. Subfigures (a)–(c) show, respectively, the spin-down, spin-up, and total current for the P configuration, and those in panels (d)–(f) are the corresponding currents for the AP configuration. The parameters are $\Gamma_0 = 0.1$, $\omega_{\mathrm{m}} = 1$, $\omega_0 = 2$, $\Omega = 0.2$, $\Omega_0 = 2$ and $g = 1.0$; and the driving detuning $\Delta = \omega_{\mathrm{d}} - \omega_0 = -1$.

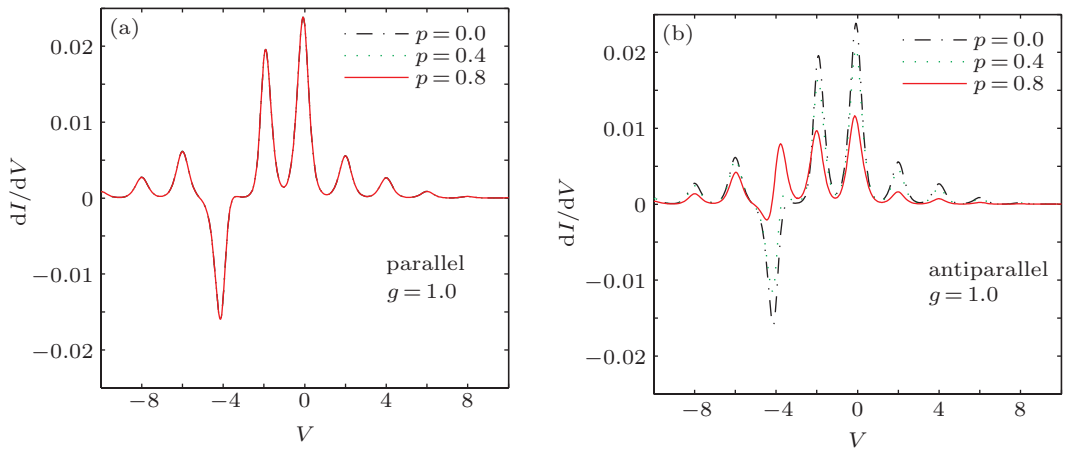


Fig. 5. (color online) Bias dependence of the differential conductance dI/dV in the (a) P and (b) AP magnetic configurations for different spin polarizations p. The parameters are the same as those in Fig. 4.

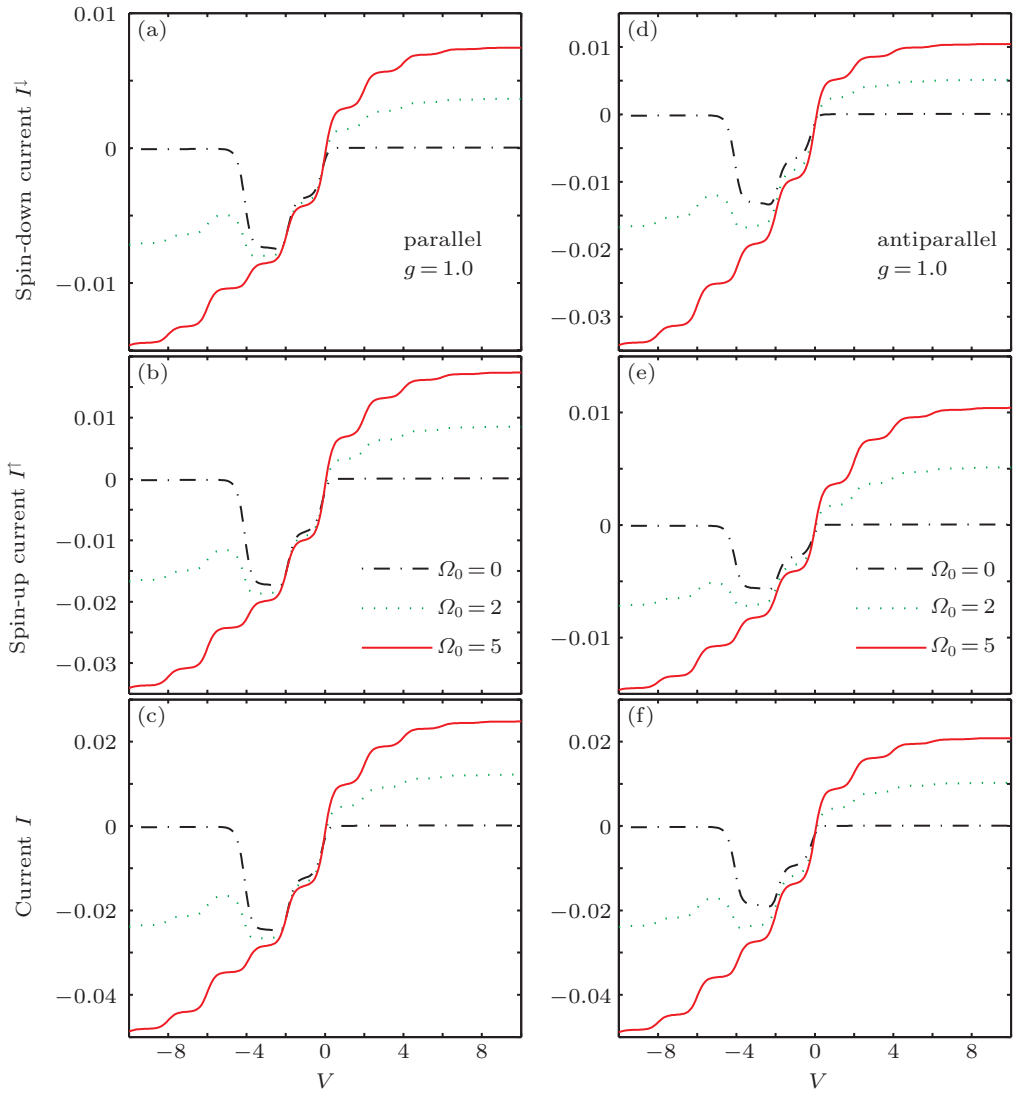


Fig. 6. (color online) Currents $I/e\omega_{\rm m}$ versus bias voltage V for different driving strengths Ω_0. Subfigures (a)–(c) show, respectively, the spin-down, spin-up, and total current for the P configuration, and those in panels (d)–(f) are the corresponding currents for the AP configuration. The parameters are $\Gamma_0 = 0.1$, $\omega_{\rm m} = 1$, $\omega_0 = 2$, $\Omega = 0.2$, $p = 0.4$, and $g = 1.0$; and the driving detuning $\Delta = \omega_{\rm d} - \omega_0 = -1$.

(iii) The relationship between transport properties and driving strength is investigated in detail. In Figs. 6(a)–6(f), the spin-down, spin-up, and total currents are plotted as a function of bias voltage V for different driving strengths Ω_0. Subfigures (a)–(c) correspond to the P configuration, and subfigures (d)–(f) correspond to the AP configuration. The main features found here are summarized as follows: for a fixed bias voltage, the currents increase toward stronger driving strength; the steps are clearer with increasing driving strength, as shown in the figures; and, when $V < -2$, the negative differential conductance is suppressed with increasing driving strength, in other words, the AC microwave field always assists the inter-dot tunneling like photon-assisted tunneling for weakly driven detuning. The $\mathrm{d}I/\mathrm{d}V$ characteristic curves are influenced by the driving strength Ω_0, which can be seen in more detail in Fig. 7.

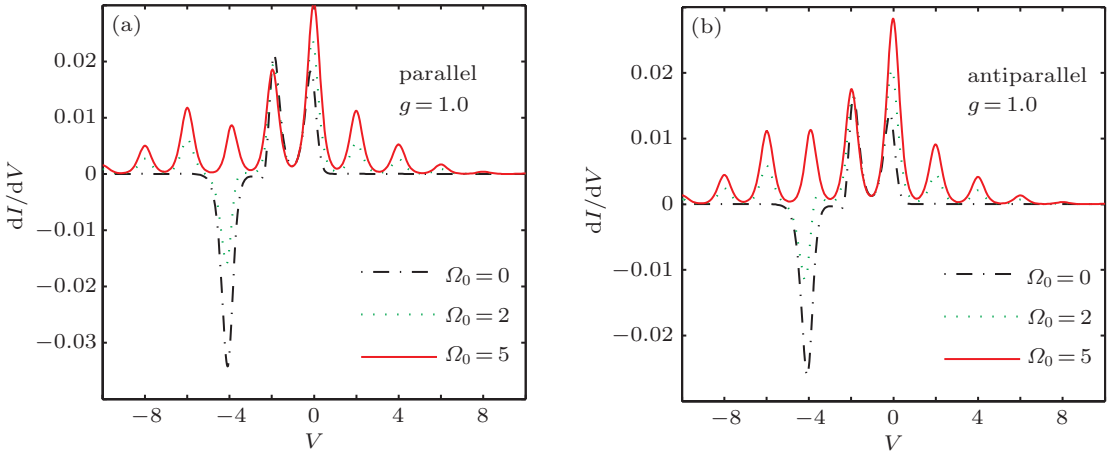


Fig. 7. (color online) Bias dependence of the differential conductance $\mathrm{d}I/\mathrm{d}V$ in the (a) P and (b) AP magnetic configurations for different driving strengths Ω_0. The parameters are the same as those in Fig. 6.

(iv) The influence of the driving detuning on the transport properties is discussed in the following. In Figs. 8(a)–8(f), the spin-down, spin-up, and total currents are plotted as functions of bias voltage V for different driving detunings Δ. Subfigures (a)–(c) correspond to the P configuration, and subfigures (d)–(f) correspond to the AP configuration. It can be seen clearly that these figures show not only the Franck–Condon steps but also negative differential conductance when the driving detuning $\Delta \neq 0$. However, when the driving frequency ω_d is equal to the energy-level splitting $\hbar\omega_0$ of DQD ($\Delta = 0$), these I–V characteristics show only the Franck–Condon steps. Besides, in the region $V < -5$ or $V > 1$, the current is always almost equal to zero when there is no AC microwave field ($\Delta = -2$) or the driving detuning is large ($\Delta = 5$). The underlying physical mechanism can be explained as follows. First, when $\Delta = -2$, there is a dynamic localization[46,47] due to the energy level difference of DQD. For a negative applied bias voltage $V = -2$, the energy level of the left (right) quantum dot is equal to the chemical potential of the left (right) lead, so the currents reach a maximum. And then, the currents quickly decrease to zero because the phonons absorb energy, which is emitted by the tunneling electron (Franck–Condon blockade). Second, for the large driving detuning ($\Delta = 5$), the tunneling currents are suppressed because of a situation like the Raman effect. Above all, the results show that a weaker driving detuning $|\Delta|$ is better for the transport. The $\mathrm{d}I/\mathrm{d}V$ characteristic curves for different driving detunings Δ are shown clearly in Fig. 9.

(v) We study the relationship between transport properties and polarization angle. The currents $I/e\omega_\mathrm{m}$ as a function of the bias voltage for different polarization angles are shown in Figs. 10(a)–10(c). Subfigures (a)–(c) show, respectively, the spin-down, spin-up, and total currents. For the collinear configurations (i.e., P ($\theta = 0$) and AP ($\theta = \pi$)), the results are presented in the previous figures. Now, the numerical results are shown for noncollinear magnetic configurations; in other words, the polarization angle varies from zero to π. First, it is clear that the spin-down current increases with the polarization angle, but the spin-up current is just the opposite. Second, with increasing polarization angle, the total current decreases significantly only in the region $-4 < V < -2$, while the total current changes very little in other regions. This anomaly results from the interplay of nonequilibrium spin accumulation in the dot. From the $\mathrm{d}I/\mathrm{d}V$ characteristic curves, it can be seen that the transport properties are influenced by the polarization angle θ in Fig. 10(d).

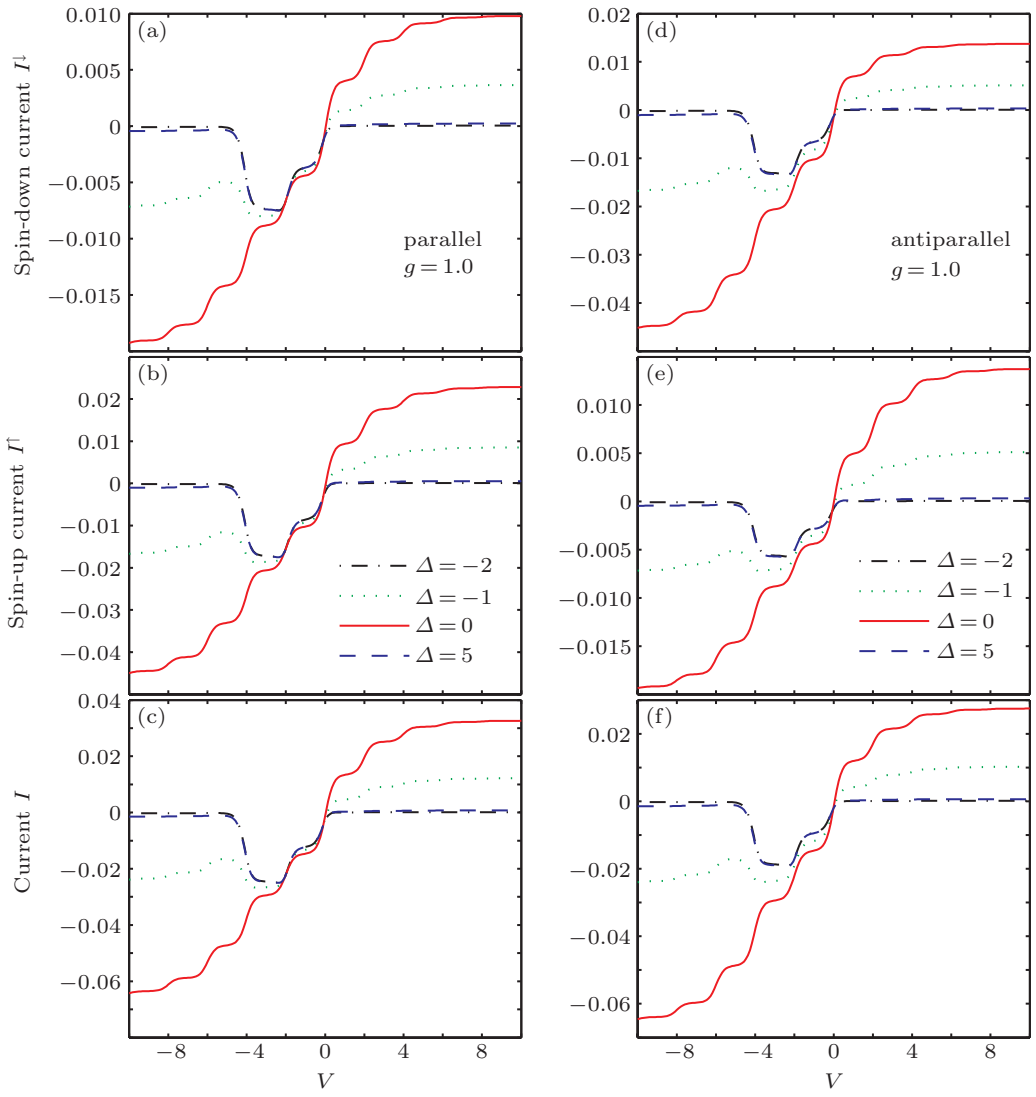


Fig. 8. (color online) Currents $I/e\omega_{\rm m}$ as a function of bias voltage V for different driving detunings Δ. Subfigures (a)–(c) show, respectively, the spin-down, spin-up, and total current for the P configuration, and those in panels (d)–(f) are the corresponding currents for the AP configuration. The parameters are $\Gamma_0 = 0.1$, $\omega_{\rm m} = 1$, $\omega_0 = 2$, $\Omega = 0.2$, $\Omega_0 = 2$, $g = 1.0$, and $p = 0.4$.

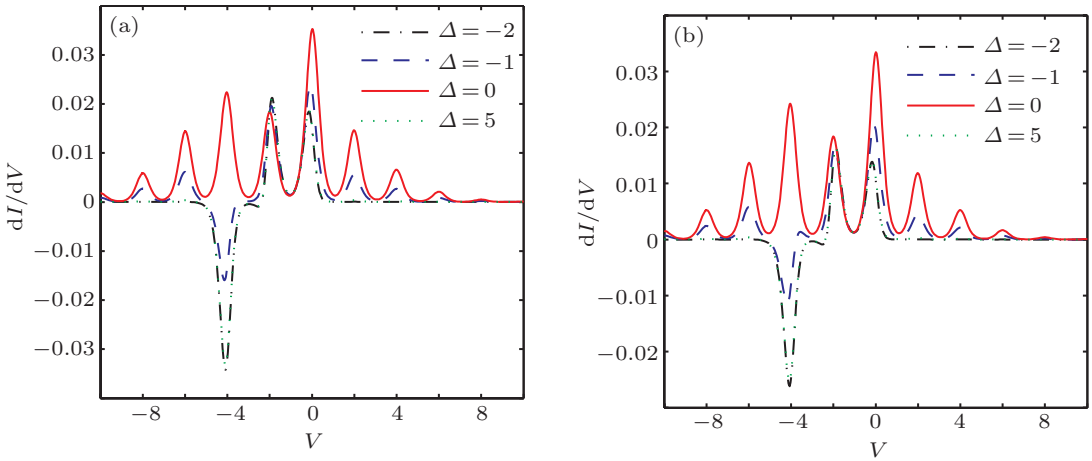


Fig. 9. (color online) Differential conductance dI/dV as a function of bias voltage V in the (a) P and (b) AP magnetic configurations for different driving detunings Δ. The parameters are the same as those in Fig. 8.

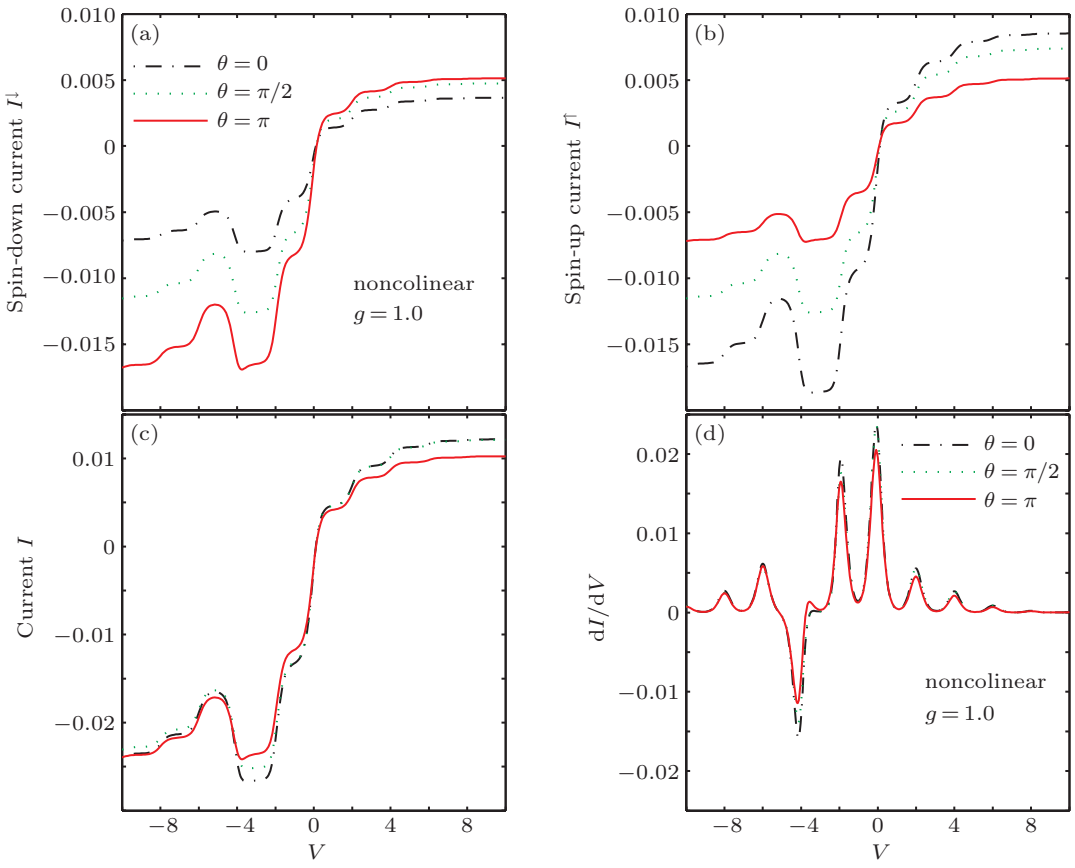


Fig. 10. (color online) Currents $I/e\omega_{\rm m}$ and differential conductance $\mathrm{d}I/\mathrm{d}V$ versus bias voltage V for different polarization angles. Subfigures (a)–(d) show, respectively, the spin-down, spin-up, total current and the differential conductance. The parameters are $\Gamma_0 = 0.1$, $\omega_{\rm m} = 1$, $\omega_0 = 2$, $\Omega = 0.2$, $\Omega_0 = 2$, $g = 1.0$, $p = 0.4$, and $\Delta = -1$.

5. Conclusion

In conclusion, we have analyzed the properties of transport through a vibrating double quantum dot coupled to noncollinear magnetized leads. The tunneling rate and the energy-level splitting of the DQD can be changed by varying the gate voltage. We apply a driving microwave field to the DQD system, and it has an effect on the transition rate. Under the driving microwave field, the electron tunneling between the DQD can be regarded as a stimulated transition or radiation that depends on the positive or negative bias voltage. In the presence of the driving microwave field and the strong electron–phonon interaction, some interesting phenomena are observed, such as a negative differential conductance and phonon-assisted tunneling occurring under certain conditions. This involves two processes: i) the tunneling electron emits a phonon leading to a decrease of the currents; and, ii) the tunneling electron absorbs a phonon giving rise to phonon-assisted tunneling. Furthermore, the spin currents depend significantly on the spin polarization in the regime of Coulomb blockade. Compared with the P configuration, in the AP configuration, the variations of the spin currents have a nonlinear relation with the spin polarization due to the Coulomb blockade. Moreover, the polarization angle has something to do with the spin polarization, which can change the tunneling rate nonlinearly.

References

[1] van der Wiel W G, de Franceschi S, Elzerman J M, Fujisawa T, Tarucha S and Kouwenhoven L P 2002 *Rev. Mod. Phys.* **75** 1
[2] Walter S, Trauzettel B and Schmidt T L 2013 *Phys. Rev. B* **88** 195425
[3] Illera S, Prades J D, Cirera A and Cornet A 2012 *Europhys. Lett.* **98** 17003
[4] Rinzan M, Jenkins G, Drew H D, Shafranjuk S and Barbara P 2012 *Nano Lett* **12** 3097
[5] Zheng X, Yan Y J and Ventra M D 2013 *Phys. Rev. Lett.* **111** 086601
[6] Dias da Silva L G G V, Vernek E, Ingersent K, Sandler N and Ulloa S E 2013 *Phys. Rev. B* **87** 205313
[7] Zhao L L, Zhao H K and Wang J 2012 *Phys. Lett. A* **376** 1849
[8] Lunde A M, López-Monís C, Vasiliadou I A, Bonilla L L and Platero G 2013 *Phys. Rev. B* **88** 035317
[9] Smit R H M, Noat Y, Untiedt C, Lang N D, van Hemert M C and van Ruitenbeek J M 2002 *Nature* **419** 906
[10] Zhitenev N B, Meng H and Bao Z 2002 *Phys. Rev. Lett.* **88** 226801
[11] Qiu X H, Nazin G V and Ho W 2004 *Phys. Rev. Lett.* **92** 206102
[12] Steele G A, Hüttel A K, Witkamp B, Poot M, Meerwaldt H B, Kouwenhoven L P and van der Zant H S J 2009 *Science* **325** 1103
[13] Lassagne B, Tarakanov Y, Kinaret J, Garcia-Sanchez D and Bachtold A 2009 *Science* **325** 1107
[14] Leturcq R, Stampfer C, Inderbitzin K, Durrer L, Hierold C, Mariani E, Schultz M G, von Oppen F and Ensslin K 2009 *Nat. Phys.* **5** 327
[15] Lambert N, Flindt C and Nori F 2013 *Europhys. Lett.* **103** 17005
[16] Santamore D H, Lambert N and Nori F 2013 *Phys. Rev. B* **87** 075422
[17] Kim S and Marzari N 2013 *Phys. Rev. B* **87** 245407
[18] Zhang S N, Pei W, Fang T F and Sun Q F 2012 *Phys. Rev. B* **86** 104513
[19] Zhang A M and Zhang Q M 2013 *Chin Phys B* **22** 087103
[20] Koch J, von Oppen F and Andreev A V 2006 *Phys. Rev. B* **74** 205438

[21] Donabidowicz-Kolkowska A and Timm C 2012 *New J. Phys.* **14** 103050
[22] Donarini A, Yar A and Grifoni M 2012 *New J. Phys.* **14** 023045
[23] Luo W, Wang R Q, Hu L B and Yang M 2013 *Chin. Phys. B* **22** 047201
[24] Luo J Y, Shen Y, He X L, Li X Q and Yan Y J 2011 *Phys. Lett. A* **376** 59
[25] He Z L, Lü T Q, Li H, Li L J, Cui L and Xue H J 2011 *Phys. Scr.* **84** 035703
[26] Peña-Aza M E, Scorrano A and Gorelik L Y 2013 *Phys. Rev. B* **88** 035412
[27] Lai W X, Cao Y S and Ma Z S 2012 *J. Phys.: Condens. Matter* **24** 175301
[28] Jiang Z T, Yu C L, Zhao R M, Lü J and Han Q Z 2011 *Phys. Rev. B* **83** 195308
[29] Muralidharan B and Grifoni M 2013 *Phys. Rev. B* **88** 045402
[30] Yang F B, Wu S Q, Yan C H, Huang R, Hou T and Bi A H 2008 *Chin. Phys. B* **17** 1383
[31] Chen X W, Chen B J, Shi Z G and Song K H 2009 *Acta Phys. Sin.* **58** 2720 (in Chinese)
[32] Xue H B, Zhang Z X and Fei H M 2012 *Eur. Phys. J. B* **85** 336
[33] Wu S Q, He Z, Yan C H, Chen X W and Sun W L 2006 *Acta Phys. Sin.* **55** 1413 (in Chinese)
[34] Wu S Q, Sun W L, Yu W L and Wang S J 2005 *Acta Phys. Sin.* **54** 2910 (in Chinese)
[35] Weymann I and Barnas J 2007 *Phys. Rev. B* **75** 155308
[36] Hornberger R, Koller S, Begemann G, Donarini A and Grifoni M 2008 *Phys. Rev. B* **77** 245313
[37] Mahan G D 2000 *Many-Particle Physics*, 3rd edn. (New York: Plenum) p. 457
[38] Song J, Sun Q F, Gao J and Xie X C 2007 *Phys. Rev. B* **75** 195320
[39] Fang T F, Sun Q F and Luo H G 2011 *Phys. Rev. B* **84** 155417
[40] Xue H B, Nie Y H, Li Z J and Liang J Q 2011 *Phys. Lett. A* **375** 716
[41] Li X Q, Cui P and Yan Y J 2005 *Phys. Rev. Lett.* **94** 066803
[42] Stoof T H and Nazarov Y V 1996 *Phys. Rev. B* **53** 1050
[43] Gurvitz S A and Prager Ya S 1996 *Phys. Rev. B* **53** 15932
[44] Koch J and von Oppen F 2005 *Phys. Rev. Lett.* **94** 206804
[45] Sapmaz S, Jarillo-Herrero P, Blanter Y M, Dekker C and van der Zant H S J 2006 *Phys. Rev. Lett.* **96** 026801
[46] Grossmann F, Dittrich T, Jung P and Hänggi P 1991 *Phys. Rev. Lett.* **67** 516
[47] Grifoni M and Hänggi P 1998 *Phys. Rep.* **304** 229